Available online at www.sciencedirect.com
SCIENCE DIRECT®
Global and Planetary Change 42 (2004) 45–58
GLOBAL AND PLANETARY CHANGE
www.elsevier.com/locate/gloplacha

Spatially distributed surface energy balance and ablation modelling on the ice cap of King George Island (Antarctica)

Matthias Braun[a,b,*], Regine Hock[c]

[a] Zentrum für Fernerkundung der Landoberfläche, Universität Bonn, Walter-Flex-Str. 3, D-53113 Bonn, Germany
[b] Institut für Physische Geographie, Universität Freiburg, Werderring 4, D-79085 Freiburg, Germany
[c] Department of Physical Geography and Quaternary Geology, Stockholm University, SE-106 91 Stockholm, Sweden

Received 12 May 2003; received in revised form 14 September 2003; accepted 21 November 2003

Abstract

Unlike continental Antarctica, snow and ice melt is a significant component of the mass balance of glacial systems on the northern Antarctic Peninsula. Over several austral summers, a comprehensive field programme was conducted on the King George Island ice cap including the operation of three automatic weather stations and ablation measurements at different altitudes. These data were used to drive a spatially distributed energy balance model to investigate melt during the period from 2 December 1997 to 12 January 1998. Averaged over the study area (418 km^2) and over this 6-week period, net radiation was found to be the main energy source (26 W m^{-2}) followed by the sensible heat flux (8 W m^{-2}). The latent heat flux was negative (-8 W m^{-2}) indicative of sublimation. High melt rates prevailed during synoptic weather conditions associated with low or even reversed temperature lapse rates. However, little melting occurred during periods of high decrease in air temperature with increasing elevation (-0.8 to -1 K 100 m^{-1}). These findings provide sufficient warning for the adoption of a constant lapse rate derived from averaged longer-term data which would significantly underestimate total melt due to underestimation of air temperatures at higher elevations during the periods when most melt occurs. Increasing air temperature by 1 and 2 K enhanced spatially averaged ablation by 27% and 62%, respectively, suggesting a high sensitivity to potential future climate warming in the area.

Keywords: Surface energy balance; Ablation; Snowmelt; Distributed modelling; Climatic change; King George Island; South Shetland Islands; Antarctica

1. Introduction

The Antarctic Peninsula is a region of on-going drastic changes in the climatic and glacial systems. Recent disintegration of ice shelves on both sides of the peninsula has raised public interest and drawn scientific attention to the region (Doake and Vaughan, 1991; Skvarca, 1993; Doake et al., 1998; Lucchita and Rosanova, 1998; Rott et al., 1998; Scambos et al., 2000; De Angelis and Skvarca, 2003). Rapid glacier retreat has been observed at various locations on the Antarctic Peninsula and in particular on King George Island (Simões and Dani, 1994; Wunderle, 1996; Kejna et al., 1998; Park et al., 1998; Simões et al.,

* Corresponding author. Zentrum für Fernerkundung der Landoberfläche, Universität Bonn, Walter-Flex-Str. 3, D-53113 Bonn, Germany. Tel.: +49-228-73-4975; fax: +49-228-73-6857.
E-mail addresses: matthias.braun@uni-bonn.de (M. Braun), regine.hock@natgeo.su.se (R. Hock).

0921-8181/$ - see front matter © 2004 Elsevier B.V. All rights reserved.
doi:10.1016/j.gloplacha.2003.11.010

1999; Braun and Goßmann, 2002). Repeated satellite image acquisitions indicated a significant upward shift of the late summer snow line on King George Island (Braun and Rau, 2001) and of the dry snow line on the Antarctic Peninsula plateau during the 1990s (Rau and Braun, 2002). Recent studies link such phenomena to the extraordinary air temperature increase and persistent warm temperatures during the 1990s observed in long-term meteorological records from permanent research stations on the peninsula (King, 1994; Smith et al., 1996; Harangozo et al., 1997; Skvarca et al., 1998). Data from King George Island reveal an average increase in air temperature of 0.031 K $year^{-1}$ during the period 1969–2002 (http://www.nbs.ac.uk/icd/gjma/temps.html). The warming trend is most significant for the summer months. Several studies have stressed a high sensitivity of the region to further warming (e.g. Knap et al., 1996; Morris, 1999).

This study is part of a comprehensive glacio-meteorological field project conducted during several summers on King George Island between 1996 and 2000. The general purpose was to investigate the coupling between climate and ablation based on detailed field measurements, satellite data and modelling approaches (Braun et al., 2000, 2001a; Braun, 2001). This paper presents results from the application of a spatially distributed surface energy balance model to compute melt rates of the ice cap of King George Island for a six-week period in 1997/1998. The specific objectives are: (1) to investigate the spatial distribution of the surface energy fluxes across the study area; (2) to test the sensitivity of modelled melt to the assumption on various model parameters; and (3) to quantify changes in glacier melt in response to temperature increase.

2. Study area

King George Island is the largest of the South Shetland Islands located at the northern tip of the Antarctic Peninsula (Fig. 1). More than 92% of its surface is ice covered (~ 1250 km^2). A major geological ridge, the Barton horst, forms the backbone of the island and subdivides the ice cap into several independent glacial systems. The top of the ice cap

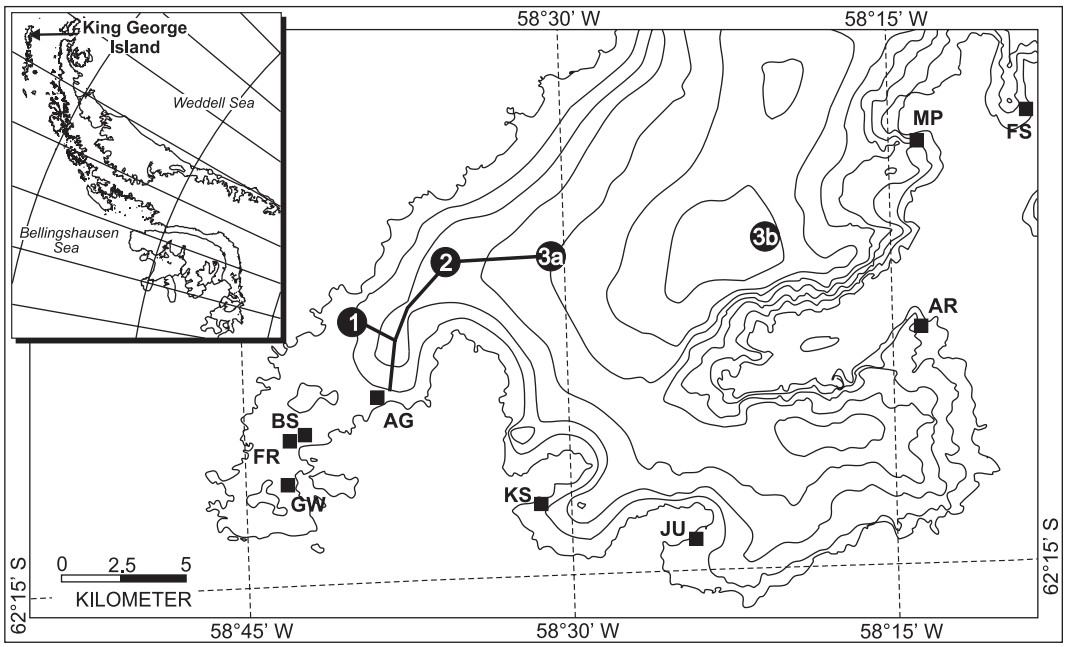

Fig. 1. Locations of automatic weather stations 1, 2, 3a, 3b and profiles of ablation measurements on the King George Island Ice Cap. Permanent research stations are denoted as follows: FR: Frei, BS: Bellingshausen, GW: Great Wall, AG: Artigas, KS: King Sejong, JU: Jubany, AR: Arctowski, MP: Machu Picchu, FS: Ferraz. Contour lines with 100 m spacing.

reaches elevations of up to 705 m a.s.l. The field measurements were conducted on the western part of the ice cap. Hence, the modelling was restricted to the ice-covered area displayed in Fig. 1. It covers an area of 418 km^2 with a maximum elevation of 679 m a.s.l. The northern slopes are gently inclined while the southern slopes are generally steep.

The climate is characterised by the frequent succession of eastward moving low-pressure centres in the circumpolar west wind zone of the Southern Hemisphere (Jones and Simmonds, 1993; Turner and Leonard, 1996). This fact and the location near the sea ice edge during winter lead to a relatively warm, maritime climate resulting in low annual variability of mean monthly air temperatures (Smith et al., 1996). Barrier winds along the east coast of the Antarctic Peninsula occasionally advect cold dry air masses towards the South Shetland Islands (Schwerdtfeger, 1984; Parish, 1983). During the summer months, air temperature at sea level rises well above 0 °C, and even the highest elevations of the ice cap are subject to melt. Snow melt generally starts in November at lower elevations and lasts until March (Wen et al., 1998), however, also during the austral winter pronounced snow melt events may occur (Rachlewizc, 1997).

Point-scale energy balance calculations indicated that at elevations around 100 m a.s.l. net radiation provided on average about 2/3 of the energy available for melt, while at higher elevations all energy gain originated from net radiation (Bintanja, 1995; Braun et al., 2001a). Melt events are strongly associated with the advection of warm humid air masses from northerly directions induced by low pressure centres passing along the northern Antarctic Peninsula and though the Drake Passage. During such meteorological situations, temperature lapse rates are low. (In the following, we refer to low lapse rates as low decreases in temperature with increasing elevation and vice versa). In contrast, easterly and southerly wind directions lead to colder air temperatures and higher, predominately dry-adiabatic lapse rates. Northerly air flow prevailed in the first and last 2 weeks of the measurement period (2 December 1997–12 January 1998) surrounding a period of cold south-easterly flow in between. The cold period was terminated by a very strong northerly advection event (Braun et al., 2001a). About 30 mm of precipitation were recorded at AWS 1 within a few days corresponding to three-quarters of total precipitation during the 6-week measurement period, and resulted in a thin new snow cover down to the lowest elevations. The mean temperature during the entire observation period was 0 °C with hourly maximum and minimum values of 3.5 and −5.5 °C, respectively.

Information about accumulation on the island is scarce and the data available are ambiguous. Stansbury (1961) and Noble (1965) conducted mass balance measurements on small cirque glaciers close to the main ice cap in the end of the 1950's. Mass balance data collected along a transect on the ice cap up to 250 m a.s.l. between 1969 and 1971 indicated steep mass balance gradients in the order of magnitude as generally found in maritime environments (Orheim and Govorukha, 1982). A comprehensive summary of the island's topographic, climatological and glaciological settings is given by Braun (2001).

3. Data base

Three automatic weather stations (AWSs) were operated on the ice cap between 2 December 1997 and 12 January 1998. Two stations were placed at 85 and 255 m a.s.l., respectively, while a third station was operated at 385 m a.s.l. but relocated to a site near the top of the study area at 620 m a.s.l. for part of the measurement period (Fig. 1). All stations were instrumented with Vector Instruments A100R wind anemometer and Vaisala HMP35C temperature and humidity sensors at two levels (0.5 and 2 m above the surface). Wind direction was measured using a Vector Instrument W200P wind vane. Net radiation balance was monitored with a Campbell Q7 net radiometer, and shortwave incoming and reflected radiation were measured using Skye SP 1110 pyranometers. The lowermost AWS was furthermore instrumented with a tipping bucket rain gauge and a Campbell SR50 sonic ranger to monitor surface elevation changes, and thus indirectly glacier melt and snow accumulation. All sensors were sampled every 10 s and data were stored as 10 min and hourly averages. The stations were visited regularly for maintenance at daily to weekly intervals depending on the weather conditions and the location of the

AWS. Riming occurred particularly at the uppermost AWS, thus affecting data quality. All data records were carefully scrutinised and potentially erroneous data, e.g. data beyond logical limits or affected by riming, were rigorously eliminated. Resulting data gaps (about 10% of data at AWS 3 and <2% at AWS1 and AWS2) were interpolated using data from the other meteorological stations.

A total of 15 bamboo stakes were drilled into the ice cap at different elevations to monitor ablation complementing the continuous ablation record at AWS1. Readings were taken regularly in connection with AWS maintenance. The stake data and the continuous snow depth record were converted into water equivalent melt (w.e.) using snow density data obtained in snow pits close to the AWSs.

Calculations were performed on a 100 m resolution digital elevation model derived from a heterogeneous data set based on contour lines from existing maps, mobile DGPS surveys in the central part of the ice cap and a coastline from a SPOT 4 XS image mosaic (Braun et al., 2001b, 2002). The ice covered area was derived from the SPOT image and the firn line was retrieved from an ERS-2 SAR image (Braun et al., 2000). To initialise the melt model, a grid with initial snow water equivalent at the modelling starting day was generated. For any grid cells containing direct measurements from snow pits measured data was used. For the remaining grid cells, snow water equivalent was distributed assuming a linear increase in accumulation with increasing elevation. The accumulation–elevation function was obtained from the data collected in snow pits at different elevations. Interpolated snow water equivalent on 2 December 1997 ranged from 85 cm w.e. at the top of the study area to 25 cm w.e. at the lowest elevations.

4. Methods

Glacier melt is computed using a distributed surface energy-balance model (Hock, 1998) driven by hourly air temperature, relative humidity, wind speed and global radiation, reflected shortwave radiation and net radiation data collected at AWS 1. Air temperature is extrapolated assuming a linear decrease with elevation. The temperature lapse rate was calculated for each time step from the data at AWS 1 and AWS 2. Relative humidity and wind speed were assumed spatially invariant. The energy available for melt Q_M is given by the formula

$$Q_M = (I + D_s + D_t)(1 - \alpha) + L_{in} + L_{out} + Q_H + Q_E + Q_G + Q_R$$

where I is direct solar radiation, D_s and D_t are diffuse sky and diffuse terrain solar radiation, respectively, α is albedo, L_{in} is longwave incoming radiation, L_{out} is longwave outgoing radiation, Q_H is the sensible heat flux, Q_E is the latent heat flux, Q_G is the ground heat flux in the ice or snow and Q_R is the energy contributed by rain. Energy fluxes directed towards the surface are taken positive, those away from the surface negative. The model puts emphasis on the computation of the radiation components. Global radiation is computed by separating measured global radiation into the direct and diffuse components. These are spatially extrapolated individually taking into account topographic effects, such as shading, slope and aspect. Ice albedo is assumed constant in space and time using the mean value derived from the measurements (0.39). Snow albedo is generated by the model for each time step and each grid cell as a function of air temperature and time since the last snowfall. Longwave incoming radiation is computed at AWS 1 from measured net radiation, the measured shortwave radiation balance and the computed outgoing longwave radiation. It is then extrapolated as a function of sky-view factor, air and surface temperature according to the parameterization suggested by Plüss and Ohmura (1997). Longwave outgoing radiation is approximated as a function of surface temperature following Stefan-Boltzmann's law. The surface temperature is set to 0 °C, if Q_M is positive. If Q_M turns negative, melt is set to zero and the surface is assumed to cool. The surface temperature is computed by lowering it iteratively until Q_M becomes zero. An iterative procedure is needed since a lower surface temperature also affects longwave radiation, the turbulent heat fluxes and the heat flux supplied by rain.

The turbulent heat fluxes are computed by the bulk aerodynamic approach based on air temperature, relative humidity and wind speed data from the 2 m level at AWS 1 as well as computed surface

temperatures. Roughness lengths were treated as tuning parameters and optimised to yield maximum agreement between measured and modelled melt. Hence, the turbulent fluxes were treated as the remainder of the energy balance and a Bowen approach was used to separate sensible and latent heat. A value of surface roughness of momentum (z_0) of 0.001 m was obtained and also assumed for the roughness lengths of heat and moisture. The heat supplied by rain is calculated as a function of rainfall rate and air temperature. Heat flux into the ice and snow is neglected.

Measured precipitation is distributed to the grid as a function of elevation and assumed to increase linearly by 10% per 100 m as derived from the meteorological records and ice core data (unpublished data). Snow and rainfall are discriminated according to a temperature divider of 1.0 °C, assuming a mixture of rain and snow for a transition zone ranging from 1 K above and 1 K below the threshold temperature. Ablation is computed from melt adjusted for the mass lost by sublimation or gained by condensation.

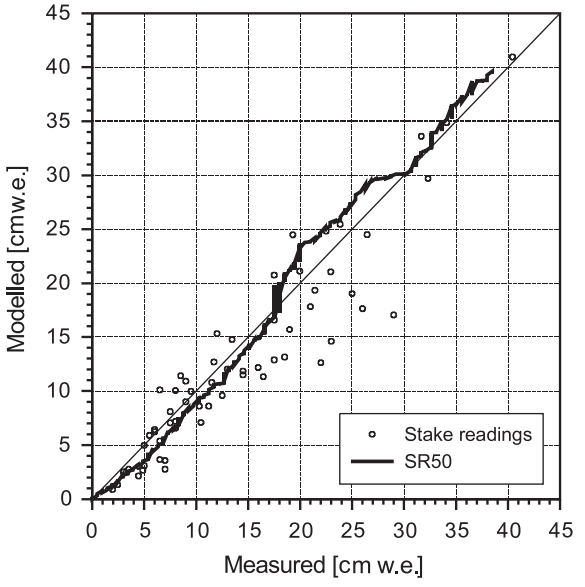

Fig. 2. Modelled versus measured cumulative melt over the period 2 December 1997 to 12 January, 1998. The thick line refers to the continuous data set derived from the SR50 sonic ranger at AWS 1 and the dots refer to stake measurements at 15 ablation stakes along the profiles shown in Fig. 1. Thin line denotes one-one-line.

Table 1
Coefficients of determination (r^2) between measured and modelled hourly radiation components for the different AWS

		Global radiation	Shortwave radiation balance	Net radiation
AWS 1	n	960	960	960
	r^2	1.0	0.90	0.81
AWS 2	n	960	960	960
	r^2	0.90	0.88	0.74
AWS 3a	n	287	287	287
	r^2	0.86	0.77	0.55
AWS 3b	n	547	547	547
	r^2	0.88	0.64	0.11

n denotes the number of data points.

The model run as described above is referred to as *control run* in the following.

5. Results and discussion

5.1. Ablation and energy balance

The model was validated by comparing model results to corresponding measurements of melt at ablation stakes and radiation components at the other weather stations. Fig. 2 indicates a generally good agreement between modelled and measured melt. Systematic discrepancies occur at a few stakes subject to high melt. This is probably due to uncertainties in initial snow cover values leading to erroneous simulation of the timing of the snow-ice transition and thus albedo. Small-scale variations of snow depth induced by crevasse patterns, wind drift or topographic effects

Table 2
Spatial maxima, minima and mean values of the energy balance components [W m^{-2}] averaged over the period of computation (02 December 1997–12 January 1998)

	I	D	G	SWR	L_{in}	L_{out}	Q_N	Q_H	Q_E	Q_R	Q_M	A
Mean	89	124	213	39	307	−319	26	8	−8	0	24	26
Max	105	142	238	108	313	−305	90	21	−1	0	104	109
Min	29	124	165	27	300	−331	15	0	−10	0	12	14

I is direct solar radiation, D is diffuse solar radiation, G is global radiation (D+I), SWR is shortwave radiation balance, L_{in} and L_{out} are incoming and outgoing longwave radiation, respectively, Q_N is net radiation, Q_H and Q_E are the sensible and latent heat fluxes, respectively, Q_R is the heat supplied by rain, Q_M energy available for melt, and A is total ablation defined as mass loss by melt and sublimation [cm w.e.].

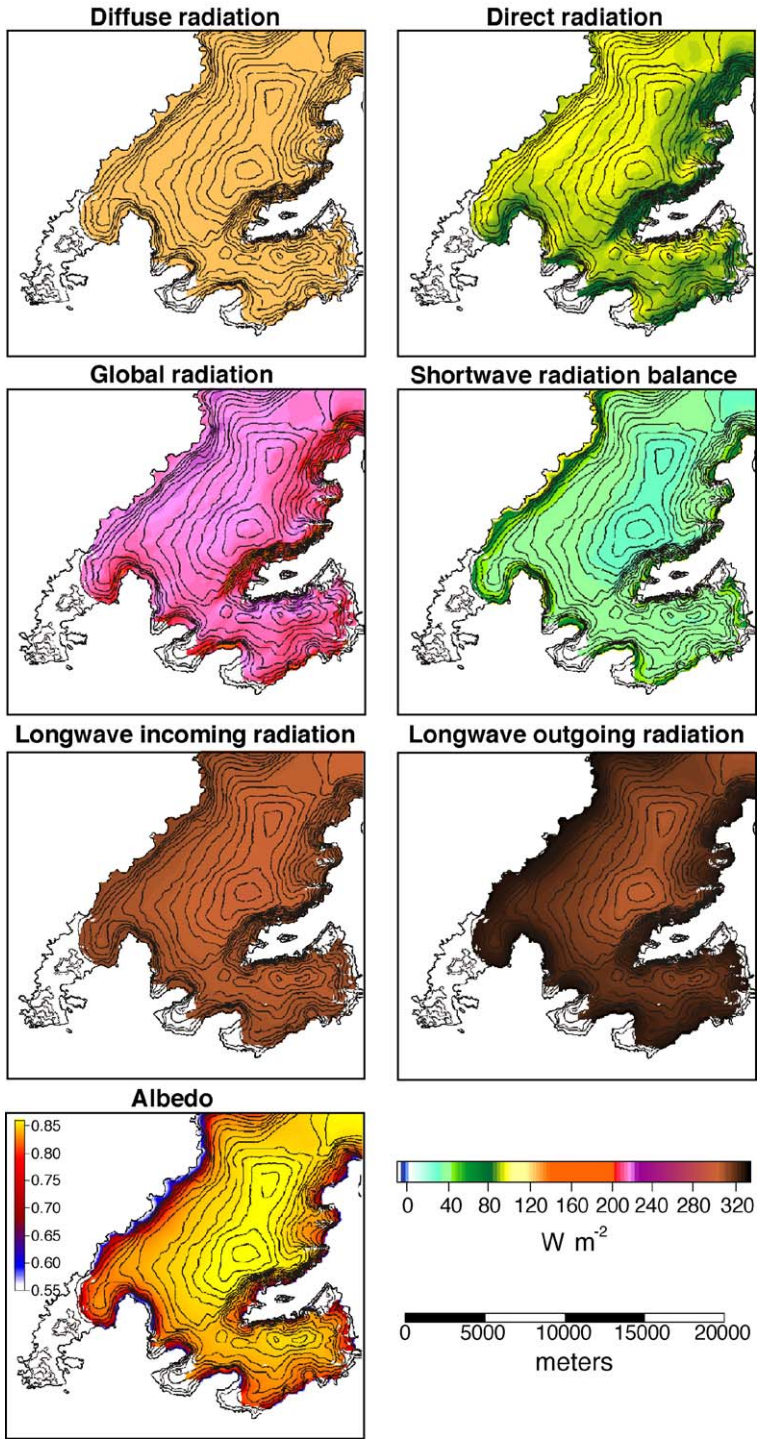

Fig. 3. Spatial variations of radiation terms averaged over the period 2 December 1997 to 12 January, 1998. Longwave outgoing radiation shown as absolute amounts. Contour lines of the surface elevation with 50 m spacing.

are neglected in the generation of the initial snow cover grid. Correlation of modelled and measured radiation components is generally high, but decreases with increasing elevation and distance from AWS 1 (Table 1). This is mainly attributed to the simplifications regarding extrapolation of air temperature, humidity

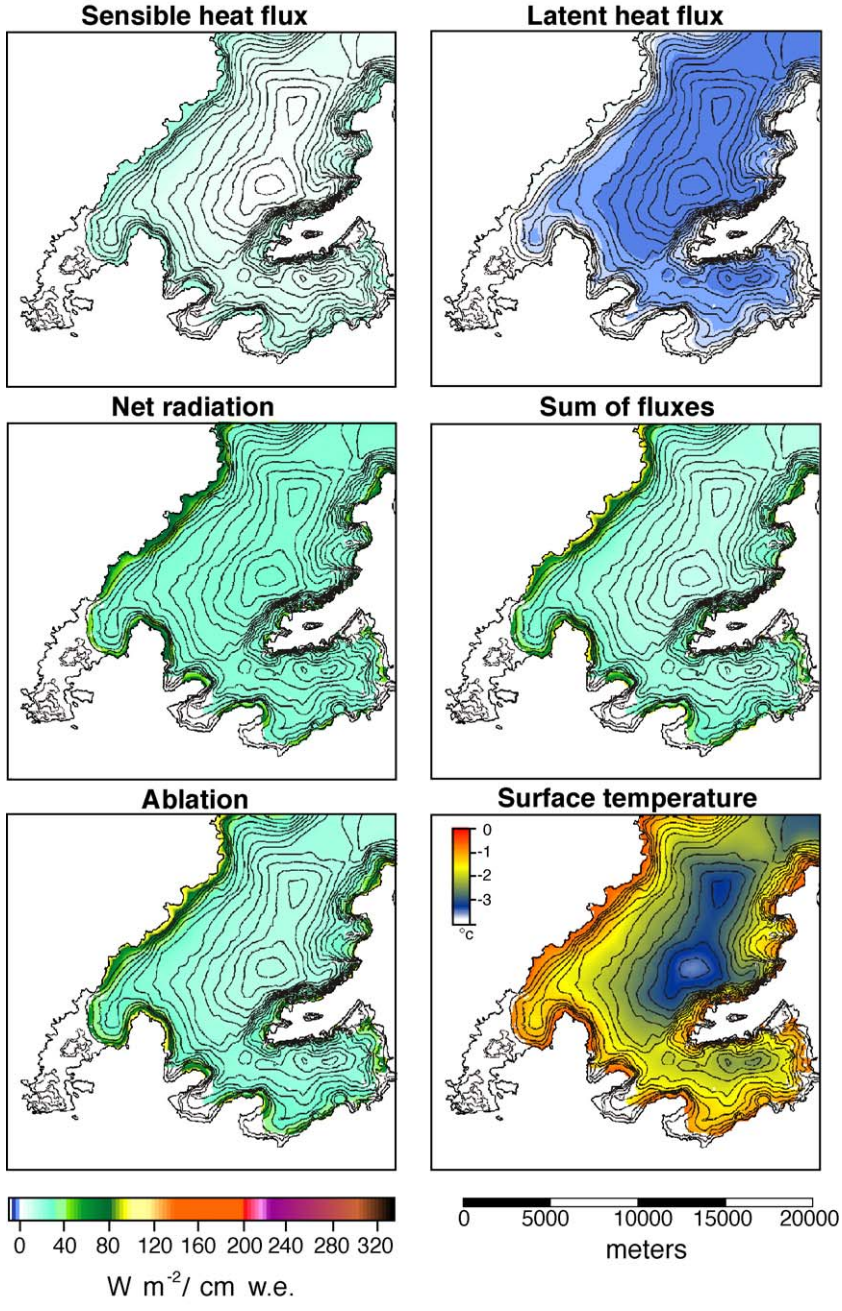

Fig. 4. Spatial distribution of surface energy balance components [W m^{-2}], ablation [cm w.e.] and surface temperature [°C] averaged over the period 2 December 1997 to 12 January, 1998. Contour lines of the surface elevation with 50 m spacing.

and wind speed, as well as the assumption of uniform cloud conditions over the study area. Despite these limitations, we consider the distributed model output as a best estimate of the surface energy balance components and melt rates, which gives the relative distribution of energy fluxes and melt rates in space and time.

Mean, maxima and minima values of the energy balance components averaged over the 6-week simulation period are given in Table 2. Net radiation is the major energy source over the entire ice cap. This is consistent with the findings of previous single location energy balance studies (Bintanja, 1995; Braun and Schneider, 2000; Braun et al., 2001a). Roughly 60% of global radiation is diffuse, confirming the observation of frequent cloudy conditions. On average, the sensible and latent heat flux are opposite in sign and balance each other. Sublimation prevails over the entire study area. Energy gain at the surface occurs by net radiation (76%) followed by the sensible heat flux (24%), while energy is consumed by melt (76%) and the latent heat flux (24%).

Figs. 3 and 4 display the spatial distribution of modelled energy balance components averaged over the 6-week simulation period. Generally, topographic influences on the radiation components are low, although the north-exposed slopes receive considerably higher global radiation than the steep south-exposed slopes. Exposition of bare glacier ice up to approximately 250 m a.s.l. by the end of the measurements period lowers albedo and leads to distinctly higher shortwave radiation balances along the margins of the ice cap compared to higher elevations, in particular along the northern margin of the ice cap where global radiation is high due to topographic effects. Longwave outgoing radiation slightly decreases with increasing elevation as a consequence of the lower mean surface temperatures at higher altitude. Surface temperatures range from -0.6 °C at the glacier margins to -3.6 °C on top of the ice cap. Both turbulent fluxes show strong altitudinal dependence resulting from the predominately negative lapse rate in air temperature.

Ablation rates show a strong dependence on elevation. Cumulative modelled ablation ranges from more than 1 m w.e. near sea level to less than 15 cm w.e. at the highest elevations. Spatially averaged total ablation reaches 26 cm during the 6-week period, corresponding to an average ablation rate of 0.65 cm/day. How much melt water runs off is unknown. Considering the surface temperature distribution, refreezing of melt water at higher elevations has to be expected, a process neglected in the model. However, we assume the amount of water refreezing to be of minor importance due to the temperate character of the firn area, as indicated by the presence of a distinct water table and the distribution of internal water inclusions in the ice cap (Jiahong et al., 1998; Pfender, 1999).

Table 3
Sensitivity analysis of the distributed energy balance model

	Parameter settings	Q_N	Q_H	Q_E	A	T_S
Control run	$z_{0,ice}=0.001$ m; $z_{0,snow}=0.001$ m $T_0=1.5$ °C; ΔP 100 m^{-1} = 10% measured hourly lapse rates, snow albedo parameterized	26	8	−8	26	−2.0
Roughness lengths	$z_{0,ice}=0.0001$ m; $z_{0,snow}=0.0001$ m	25	4	−5	23	−1.9
	$z_{0,ice}=0.01$ m; $z_{0,snow}=0.01$ m	30	21	−12	37	−2.1
	$z_{0,ice}=0.001$ m; $z_{0,snow}=0.01$ m	30	20	−11	36	−2.1
	$z_{0,ice}=0.001$ m; $z_{0,snow}=0.0001$ m	25	4	−5	23	−1.9
Precipitation	$T_0=1.0$ °C; ΔP 100 m^{-1} = 10%	28	7	−8	27	−2.0
	$T_0=2.0$ °C; ΔP 100 m^{-1} = 10%	26	8	−8	25	−2.0
	$T_0=1.5$ °C; ΔP 100 m^{-1} = 30%	24	9	−7	25	−2.1
	$T_0=1.5$ °C; ΔP 100 m^{-1} = 0%	29	6	−9	27	−1.9
Snow albedo	0.7 (constant in space and time)	34	6	−9	31	−1.9
	0.9 (constant in space and time)	13	11	−6	17	−2.2
Lapse rate	−0.2 K 100 m^{-1}	23	12	−6	29	−1.3
	−0.4 K 100 m^{-1}	21	9	−8	22	−1.6
	−0.6 K 100 m^{-1}	21	7	−9	18	−1.9
	−0.8 K 100 m^{-1}	22	5	−10	16	−2.3

Listed are values averaged over the study area and the period 02 December 1997 to 12 January 1998: net radiation, Q_N, sensible heat flux, Q_H, latent heat flux, Q_E (W m^{-2}) and surface temperature T_S (°C). A is spatially averaged total ablation (cm w.e.). z_0 denotes the roughness lengths for momentum, heat and moisture, T_0 the threshold temperature for snow–rain transition, ΔP 100 m^{-1} the precipitation change with increasing elevation.

5.2. Parameter sensitivity

Model sensitivity was investigated by systematically varying various model input parameters. The effects of altered roughness lengths, precipitation parameters, albedo and air temperatures lapse rates on energy balance components and modelled glacier melt are shown in Table 3. Previous studies have shown a large sensitivity of energy balance results to the choice of roughness lengths (e.g. Hock and Holmgren, 1996). This poses a problem since roughness lengths are difficult to obtain and to extrapolate and reported values over snow and ice cover a range of orders of magnitude (Hock, 1998). We considered a 10-fold increase and decrease in roughness lengths compared to the optimized values in addition to changes in the ratio between the values over snow and ice. Results show a considerable sensitivity of results to the assumptions on roughness lengths. Using $z_0 = 1$ cm instead of $z_0 = 1$ mm, the sensible heat flux is almost tripled. The energy loss by sublimation is only doubled, hence, there is a net increase in the turbulent fluxes. Also net radiation is increased resulting from exposure of more bare ice due to enhanced melt rates. Varying the roughness lengths for ice surfaces lead only to marginal changes in model output. This can be attributed to the fact that ice surfaces were restricted to a comparable small area skirting the glacier.

A variation of the precipitation–elevation relationship and the threshold temperature discriminating snow and rain has relatively little impact on the model results since total precipitation during the computation period was small. Changes in threshold temperature lead to slightly changed surface conditions and altered the energy fluxes via changes in albedo, rather than by a direct effect on the rain-heat flux.

Due to the large relative importance of net radiation in the energy balance, snow albedo was expected to be a sensitive variable. Several runs assuming snow albedo constant in space and time were performed adopting values within the range generally reported for snow (Paterson, 1994). Varying snow albedo between 0.7 and 0.9 results in a 19% overestimation and a 35% underestimation of ablation, respectively, compared to the control run simulations based on internal space-time variable generation of snow albedo. High sensitivity to albedo agrees with the wealth of energy balance studies emphasizing the importance of albedo for melt calculations (e.g. Oerlemans and

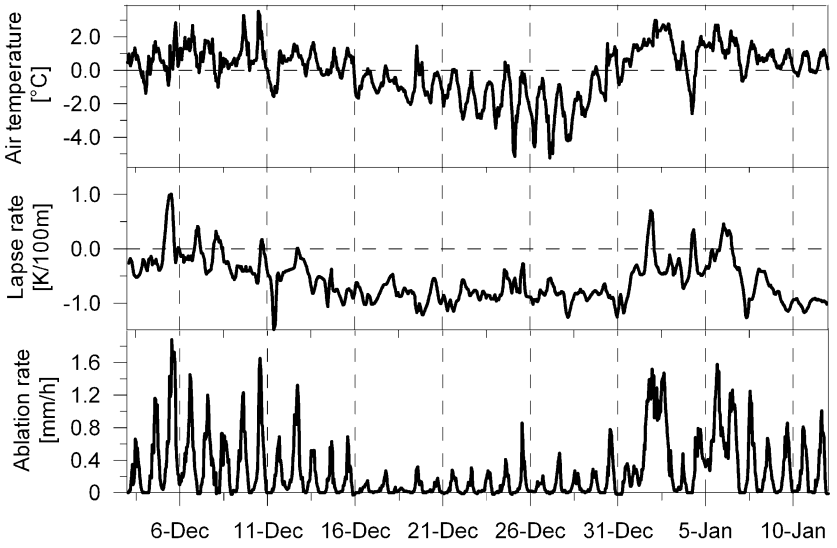

Fig. 5. Hourly values of air temperature at AWS 1, temperature lapse rate derived from data at AWS 1 (85 m a.s.l.) and AWS 2 (255 m a.s.l.), and ablation averaged over the study area.

Hoogendorn, 1989). Ice albedo turned out to be insensitive, however, resulting from the small portion of bare ice. Importance of ice albedo increases with exposure of bare glacier ice in the course of the season, or in case of future climate warming when a large portion of bare glacier ice has to be expected due to augmented melt rates.

Perhaps most striking is the sensitivity of the model to the choice of air temperature lapse rates. In contrast to deriving the lapse rate for every hour from the data at different elevations, we applied various constant lapse rates as often done in mass balance modelling (e.g. Hock, 1998). Applying a lapse rate of -0.6 K 100 m^{-1} corresponding to the average lapse rate during the simulation period results in reduction of modelled ablation by one third (Table 3). A lapse rate of roughly -0.25 K 100 m^{-1} is needed to generate the melt obtained in the control run. This stresses the strong dependence of snowmelt and lapse rates on the predominant air mass advection on King George Island (Braun et al., 2001a) and the need to adjust lapse rates to the prevailing weather situation. During cold conditions associated with easterly and southerly flows, melt rates are low, but lapse rates tend to be very high approaching -1 K 100 m^{-1} (see second half of December in Fig. 5). Conversely, during northwesterly advection of warm humid air masses, melt rates increase considerably and lapse rates are low or even reversed (e.g. first December week and beginning of January in Fig. 5). It is obvious that employment of a constant lapse rate averaged over a period including occurrence of both circulation patterns will underestimate temperature at higher elevation and thus melt. Hence, assuming average lapse rates reported in previous studies (Table 4) can be misleading since these values refer to longer-term, averaged conditions rather than to shorter-term advection events when most of the melt occurs. Accurate lapse rate are also important in degree-day melt modelling where degree-day factors are often obtained from optimization procedures (Hock, 2003). Overestimation of lapse rates will then be compensated by high degree-day factors hence invoking an overestimation in temperature sensitivity of the model. Only the employment of actual lapse rates can accommodate the variability in lapse rates, and is thus a prerequisite for accurate ablation estimates under the current climatic conditions on King George Island.

Table 4
Air temperature lapse rates along the Antarctic Peninsula

Location	Temperature lapse rate [K 100 m^{-1}]	Database	Reference
AP	−0.68	10-m snow temperatures	Martin and Peel (1978)
WAP	−0.57	10-m snow temperatures (0–1060 m)	Reynolds (1981)
WAP	−0.61	(0–2160 m)	
EAP	−0.57	(0–1060 m)	
JRI	−0.58	10-m snow temperatures	Aristarain et al. (1987)
AP	−0.57	10-m snow temperatures, meteorologcial data	Morris and Vaughan (1994)
WAP	−0.82		
EAP	0.008		
KGI	−0.79 (0 to 255 m a.s.l., summer) −0.66 (0 to 255 m a.s.l., winter)	meteorological data (1991/1992)	Wen et al. (1994)
KGI	−0.62	23 balloon soundings up to 1000 m (1990/1991)	Bintanja (1995)
KGI	−0.58 (84–255 m a.s.l.) −0.66 (84–619 m a.s.l.)	meteorological data (1997/1998)	this study

AP: Antarctic Peninsula, WAP: West Antarctic Peninsula, EAP: East Antarctic Peninsula, JRI: James Ross Island, KGI: King George Island.

5.3. Temperature sensitivity

To provide some insight into the response of the ice cap to climate warming simple temperature sensitivity experiments were conducted. The model was re-run shifting the measured temperature record and comparing results to those of the control run. The results must be treated with caution, since any other changes in meteorological variables accompanied by climate warming, such as precipitation, frequency of weather systems and radiation feedback processes, are not considered.

The effects on surface energy balance and melt are shown in Table 5. A temperature rise by 0.5, 1

Table 5
Effect of temperature increase on surface energy balance and ablation rates on King George Island based on the data set from 1997/1998

Model run		Q_N	Q_H	Q_E	A	T_S
Control run	–	26	8	−8	26	−2.0
Air temperature increase	+0.5 K	31	7	−8	29	−2.1
	+1.0 K	33	7	−8	33	−2.2
	+2.0 K	37	11	−6	42	−2.0

Energy balance components (net radiation, Q_N, sensible heat flux, Q_H, latent heat flux, Q_E) are in W m^{-2}, ablation (A) in cm w.e.

and 2 K enhances spatially averaged melt over the simulation period by 12%, 27% and 62%, respectively. This is considerably larger than the 15% increase obtained for a 1 K temperature increase at a low elevation site on King George Island (Bintanja, 1995). Net radiation increases at a higher rate than the turbulent fluxes, which can be attributed to increased bare ice area and associated albedo changes. A significant increase in ice-exposed area in response to enhanced air temperatures is illustrated in Fig. 6. The bare ice area increases from 12% at the end of the simulation period in the control run to almost 30% in the +2 K-experiment.

6. Conclusions and outlook

A distributed energy balance melt model was applied to the western part of the ice cap on King George Island (418 km^2) over the period 2 December 1997 to 12 January 1998. The model was forced by hourly data collected at meteorological stations on the glacier. Good agreement between modelled and measured ablation could be obtained with an appropriate choice of surface roughness lengths. Ablation and radiation measurements were used to validate the model. Considering the size of the study area it is obvious that more data are desirable to confirm model results and to provide better input data on initial snow cover. The need for more mass balance surveys has also been pointed out by Weidick and Morris (1998). Nevertheless, results provide valuable insight into the spatial distribution of energy fluxes and melt over a large fraction of the ice cap. Averaged over the study area total ablation modelled over the 6-week simulation period was 26 cm. Most of the energy gain was provided by net radiation (26 W m^{-2}) followed by the sensible heat flux (8 W m^{-2}). The latent heat flux was negative (−8 W m^{-2}) indicating sublimation.

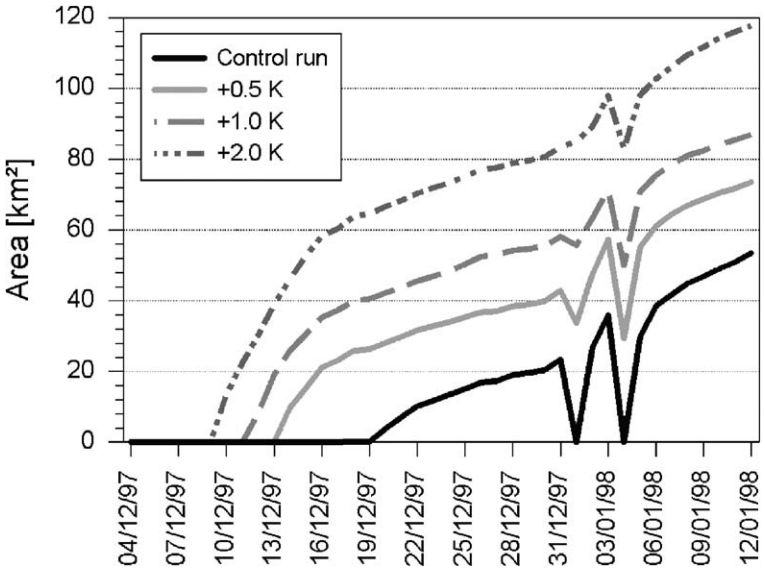

Fig. 6. Modelled area of bare ice based on measured meteorological data (control run) and in response to shifting the measured air temperature record by 0.5, 1.0 and 2.0 K. The modelled area covers 418 km^2. The increase in bare ice area as the melt season proceeds is interrupted by two major snow fall events in the beginning of January due to strong northerly advection covering the entire study area by snow.

The most striking feature was the sensitivity of results to the assumption on lapse rates. Lapse rates are very high reaching ca. −0.8 to −1 K 100 m^{-1} during periods of low melt associated with south-easterly atmospheric flow and cold air masses. High melt rates are induced by north-westerly advection of warm, moist air, and lapse rates are low or even reversed under these conditions. Lapse rates on King George Island roughly switch between these two modes depending on the synoptic weather situation. Reported average lapse rates for the western Antarctic Peninsula generally range from −0.57 to −0.82 K 100 m^{-1} (Table 4). It is obvious that assuming a constant lapse rate derived from reported average values will lead to erroneous melt simulations, since lapse rates are considerably lower during the periods when most melt occurs. Consequently, the variability in lapse rates has to be taken into account for accurate melt predictions in this area. It also follows that changes in melt rates will depend on changes in the frequency in occurrence of the prevailing two contrasting synoptic weather patterns. This poses a problem to simulating the response of glacier melt on King George Island to future climate change since changes in atmospheric circulation are difficult to predict.

Simple model experiments indicated that melt is significantly enhanced when the temperature is increased by 0.5–2 K suggesting a high sensitivity of the King George Island ice cap to climate warming. More sensitivity experiments incorporating predicted changes on other variables than temperature are needed to provide realistic estimates of the future evolution of the mass balance of King George Island.

Acknowledgements

The authors would like to thank Jefferson Simões and his group from the Laboratório de Pesquisas Antárticas e Glaciológicas, Universidad Federal do Rio Grande do Sul, Porto Alegre, Brazil for their support during field work and the pleasant atmosphere in the glacier camps. The Brazilian Antarctic Program (PROANTAR) and the Alfred-Wegener-Institut (AWI) kindly provided logistic support for the fieldwork. Funding was provided by the DFG research project (SA 694/1-1/2, SA 694/2-1). Thanks to Alun Hubbard, Anne Le Brocq and two anonymous reviewers for useful scomments on the manuscript.

References

Aristarain, A.J., Pinglot, J.F., Pourchet, M., 1987. Accumulation and temperature measurements on the James Ross Island ice cap, Antarctic Peninsula, Antarctica. Journal of Glaciology 33 (115), 1–6.

Bintanja, R., 1995. The local surface energy balance of the Ecology Glacier, King George Island, Antarctica: measurements and modelling. Antarctic Science 7 (3), 315–325.

Braun, M., 2001. Ablation on the ice cap of King George Island (Antarctica). An approach from field measurements, modelling and remote sensing. PhD thesis at the Faculty of Geosciences at the University of Freiburg, Germany. 165 pp., http://www.freidok.uni-freiburg.de/volltexte/223/.

Braun, M., Goßmann, H., 2002. Glacial changes in the area of Admiralty Bay and Potter Cove, King George Island, Antarctica. In: Beyer, M., Boelter, M. (Eds.), GeoEcology of Terrestrial Antarctic Oases. Springer Verlag, Berlin-Heidelberg, pp. 75–89.

Braun, M., Rau, F., 2001. Using a multi-year data archive of ERS SAR imagery for monitoring firn line positions and ablation patterns on the King George Island ice cap (Antarctica). In: Wunderle, S., Nagler, T. (Eds.), Proceedings of the 2nd EARSeL Workshop "Remote Sensing of Land Ice and Snow", Dresden, 16–17 June 2000, CD-ROM.

Braun, M., Schneider, C., 2000. Characteristics of summertime energy balance along the west coast of the Antarctic Peninsula. Annals of Glaciology 31, 179–183.

Braun, M., Rau, F., Saurer, H., Goßmann, H., 2000. Development of radar glacier zones on the King George Island ice cap, Antarctica, during the austral summer 1996/97 as observed in ERS-2 SAR data. Annals of Glaciology 31, 357–363.

Braun, M., Saurer, H., Vogt, S., Simões, J.C., Goßmann, H., 2001a. The influence of large-scale circulation on surface energy balance on the King George Island ice cap. International Journal of Climatology 21 (1), 21–36.

Braun, M., Simões, J.C., Vogt, S., Bremer, U.F., Blindow, N., Pfender, M., Saurer, H., Aquino, F.E., Ferron, F.A., 2001b. An improved topographic database for King George Island—Compilation, Application and Outlook. Antarctic Science 13 (1), 41–52.

Braun, M., Simões, J.C., Vogt, S., Bremer, U.F., Saurer, H., Aquino, F.E., 2002. A new satellite image map of King George Island (South Shetland Islands, Antarctica). Polarforschung 71, 47–48.

De Angelis, H., Skvarca, P., 2003. Glacier surge after ice shelf collapse. Science 299, 1560–1562.

Doake, C.S.M., Vaughan, D.G., 1991. Rapid disintegration of Wordie Ice Shelf in response to atmospheric warming. Nature 350, 328–330.

Doake, C.S., Corr, H.F.J., Rott, H., Skvarka, P., Young, N.W., 1998. Breakup and conditions for stability of the northern Larsen Ice Shelf, Antarctica. Nature 391, 778–780.

Harangozo, S.A., Colwell, S.R., King, J.C., 1997. An analysis of a 34-year air temperature record from Fossil Bluff (71°S, 68°W), Antarctica. Antarctic Science 9 (3), 355–363.

Hock, R., 1998. Modelling of glacier melt and discharge. In: Zürcher Geographische Schriften, vol. 70. ETH, Zürich, 126 pp.

Hock, R., 2003. Temperature-index modelling in mountainous areas. Journal of Hydrology 282 (1–4), 104–115.

Hock, R., Holmgren, B., 1996. Some aspects of energy balance and ablation of Storglaciären, Sweden. Geografiska Annaler 78A (2–3), 121–131.

Jiahong, W., Jiacheng, K., Jiankang, H., Zichu, X., Leibao, L., Wang, D., 1998. Glaciological studies on the King George Island ice cap, South Shetland Islands, Antarctica. Annals of Glaciology 27, 105–109.

Jones, D.A., Simmonds, I., 1993. A climatology of Southern Hemisphere extratropical cyclones. Climate Dynamics 9, 131–145.

Kejna, M., Láska, K., Caputa, Z., 1998. Recession of the Ecology Glacier (King George Island) in the period 1961–1996. In: Glowacki, P., Bednarek, J. (Eds.), Polish Polar Studies. 25th International Polar Symposium, Warsaw, 1998. Institute of Geophysics of the Polish Academy of Sciences, Warsaw, pp. 121–128.

King, J.C., 1994. Recent climate variability in the vicinity of the Antarctic Peninsula. International Journal of Climatology 14, 357–369.

Knap, W.H., Oerlemans, J., Cadée, M., 1996. Climate sensitivity of the ice cap of King George Island, South Shetland Islands, Antarctica. Annals of Glaciology 23, 154–159.

Lucchita, B.K., Rosanova, C.E., 1998. Retreat of northern margins of George VI and Wilkins Ice Shelves, Antarctic Peninsula. Annals of Glaciology 27, 41–46.

Martin, P.J., Peel, D.A., 1978. The spatial distribution of 10 m temperatures in the Antarctic Peninsula. Journal of Glaciology 20 (83), 311–317.

Morris, E.M., 1999. Surface ablation rates on Moraine Corrie Glacier, Antarctica. Global and Planetary Change 22, 221–231.

Morris, E.M., Vaughan, D.G., 1994. Snow surface temperatures in West Antarctica. Antarctic Science 6 (4), 529–535.

Noble, H.M., 1965. Glaciological observations at Admiralty Bay, King George Island, in 1957–58. British Antarctic Survey Bulletin 5 (41), 1–11.

Oerlemans, J., Hoogendorn, N.C., 1989. Mass-balance gradients and climate change. Journal of Glaciology 35 (121), 399–405.

Orheim, O., Govorukha, L.S., 1982. Present-day glaciation in the South Shetland Islands. Annals of Glaciology 3, 233–238.

Parish, T.R., 1983. The influence of the Antarctic Peninsula on the wind field over the western Weddell Sea. Journal of Geophysical Research 88 (C4), 2684–2692.

Park, B.-K., Chang, S.-K., Yoon, H.I., Chung, H., 1998. Recent retreat of ice cliffs, King George Island, South Shetland Islands, Antarctic Peninsula. Annals of Glaciology 27, 633–635.

Paterson, W.S.B., 1994. The Physics of Glaciers, Third edition. Elsevier, Oxford, 480 pp.

Pfender, M. 1999. Topographie und Glazialhydrologie von King George Island, Antarktis. Unpublished Diploma Thesis, University of Münster.

Plüss, C., Ohmura, A., 1997. Longwave radiation on snow-covered mountainous surfaces. Journal of Applied Meteorology 36 (6), 818–824.

Rachlewizc, G., 1997. Mid-winter thawing in the vicinity of Arctowski Station, King George Island. Polish Polar Research 18 (1), 15–24.

Rau, F., Braun, M., 2002. The regional distribution of the dry-snow zone on the Antarctic Peninsula north of 70°S. Annals of Glaciology 34, 95–100.

Reynolds, J.M., 1981. The distribution of mean annual temperatures in the Antarctic Peninsula. British Antarctic Survey Bulletin 54, 123–133.

Rott, H., Rack, W., Nagler, T., Skvarca, P., 1998. Climatically induced retreat and collapse of northern Larsen Ice Shelf, Antarctic Peninsula. Annals of Glaciology 27, 86–92.

Scambos, T.A., Hulbe, C., Fahnestock, M., Bohlander, J., 2000. The link between climate warming and break-up of ice-shelves in the Antarctic Peninsula. Journal of Glaciology 46 (154), 516–530.

Schwerdtfeger, W., 1984. Weather and Climate of the Antarctic. Elsevier, Amsterdam.

Simões, J.C., Dani, R., 1994. Levantamento e monitoramento de geleiras de pequeno porte: Península Keller, Ilha Rei Jorge, Antártica. Boletim de Resumos Expandidos, 38° Congreso Brasileiro de Geologia. Camboriú-SBG-SC, 349–351.

Simões, J.C., Bremer, U.F., Aquino, F.E., Ferron, F.A., 1999. Morphology and variations of glacial drainage basins in the King George Island ice field, Antarctica. Annals of Glaciology 29, 220–224.

Skvarca, P., 1993. Fast recession of the northern Larsen Ice Shelf monitored by space images. Annals of Glaciology 17, 317–321.

Skvarca, P., Rack, W., Rott, H., Ibarzábal y Donángelo, T., 1998. Evidence of recent climatic warming on the eastern Antarctic Peninsula. Annals of Glaciology 27, 628–632.

Smith, R.C., Stammerjohn, S.E., Baker, K.S., 1996. Surface air temperature variations in the western Antarctic Peninsula region. Antarctic Research Series 70, 105–121.

Stansbury, M.J., 1961. Glaciological observations at Admiralty Bay (Lat. 62°05′S, Lon. 58°24′W), King George Island, South Shetland Islands, 1959–60. Falkland Islands Dependencies Survey, Preliminary Glaciological Report 4. 45 pp. (BAS Archives Document Reference: AD6/2/1961/S5).

Turner, J., Leonard, S., 1996. Synoptic scale weather systems around the Antarctic Peninsula from satellite imagery and model fields. 8th Conference on Satellite Meteorology and Oceanography, January 28–February 02 1996, Atlanta, Georgia. American Meteorological Society, Boston, MA, pp. 574–577.

Weidick, A., Morris, E.M., 1998. Local glaciers surrounding the continental ice sheets. In: Haeberli, W., Hoelzle, M., Suter, S. (Eds.), Into the Second Century of World-Wide Glacier Monitoring—Prospects and Strategies. Studies and Reports in Hydrology, vol. 56. UNESCO, Paris, pp. 197–207.

Wen, J., Kang, J., Xie, Z., Han, J., Lluberas, A., 1994. Climate, mass balance and glacial changes on small dome of Collins ice cap, King George Island, Antarctica. Antarctic Research 5 (1), 52–61.

Wen, J., Kang, J., Han, J., Xie, Z., Liu, L., Wang, D., 1998. Glaciological studies on King George Island ice cap, South Shetland Islands, Antarctica. Annals of Glaciology 27, 105–109.

Wunderle, S., 1996. Die Schneedeckendynamik der Antarktischen Halbinsel und ihre Erfassung mit aktiven und passiven Fernerkundungsverfahren. Freiburger Geographische Hefte 48 (172 pp.).